Designing a space-based galaxy redshift survey to probe dark energy

Yun Wang,[1]★ Will Percival,[2] Andrea Cimatti,[3] Pia Mukherjee,[4] Luigi Guzzo,[5]
Carlton M. Baugh,[6] Carmelita Carbone,[3] Paolo Franzetti,[7] Bianca Garilli,[7]
James E. Geach,[6] Cedric G. Lacey,[6] Elisabetta Majerotto,[5] Alvaro Orsi,[6] Piero Rosati,[8]
Lado Samushia[2,9] and Giovanni Zamorani[10]

[1]*Homer L. Dodge Department of Physics and Astronomy, University of Oklahoma, 440 W Brooks St., Norman, OK 73019, USA*
[2]*Institute of Cosmology and Gravitation, University of Portsmouth, Dennis Sciama Building, Portsmouth P01 3FX*
[3]*Dipartimento di Astronomia, Alma Mater Studiorum – Università di Bologna, Via Ranzani 1, I-40127 Bologna, Italy*
[4]*Sussex Astronomy Centre, Department of Physics and Astronomy, University of Sussex, Falmer, Brighton BN1 9QH*
[5]*INAF – Osservatorio di Brera, Via Bianchi 46, I-23807 Merate, Italy*
[6]*Institute for Computational Cosmology, Physics Department, Durham University, South Road, Durham DH1 3LE*
[7]*INAF, IASF-Milano, Via Bassini 15, 20133 Milano, Italy*
[8]*European Southern Observatory, Karl Schwarzschild Strasse 2, D-85748 Garching bei Muenchen, Germany*
[9]*National Abastumani Astrophysical Observatory, Ilia State University, 2A Kazbegi Ave, GE-0160 Tbilisi, Georgia*
[10]*INAF – Osservatorio Astronomico di Bologna, Via Ranzani 1, I-40127 Bologna, Italy*

ABSTRACT

A space-based galaxy redshift survey would have enormous power in constraining dark energy and testing general relativity, provided that its parameters are suitably optimized. We study viable space-based galaxy redshift surveys, exploring the dependence of the Dark Energy Task Force (DETF) figure-of-merit (FoM) on redshift accuracy, redshift range, survey area, target selection and forecast method. Fitting formulae are provided for convenience. We also consider the dependence on the information used: the full galaxy power spectrum $P(k)$, $P(k)$ marginalized over its shape, or just the Baryon Acoustic Oscillations (BAO). We find that the inclusion of growth rate information (extracted using redshift space distortion and galaxy clustering amplitude measurements) leads to a factor of ∼3 improvement in the FoM, assuming general relativity is not modified. This inclusion partially compensates for the loss of information when only the BAO are used to give geometrical constraints, rather than using the full $P(k)$ as a standard ruler. We find that a space-based galaxy redshift survey covering ∼20 000 deg^2 over $0.5 \lesssim z \lesssim 2$ with $\sigma_z/(1 + z) \leq 0.001$ exploits a redshift range that is only easily accessible from space, extends to sufficiently low redshifts to allow both a vast 3D map of the universe using a single tracer population, and overlaps with ground-based surveys to enable robust modelling of systematic effects. We argue that these parameters are close to their optimal values given current instrumental and practical constraints.

Key words: cosmology: observations – distance scale – large-scale structure of Universe.

1 INTRODUCTION

More than a decade after the discovery of cosmic acceleration (Riess et al. 1998; Perlmutter et al. 1999), its cause (dubbed 'dark energy' for convenience) remains shrouded in mystery. While current observational data are consistent with dark energy being a cosmological constant (e.g. Wang & Tegmark 2004; Wang 2009), the uncertainties are large, and do not rule out models with dynamical scalar fields (see e.g. Freese et al. 1987; Linde 1987; Peebles & Ratra 1988;

Wetterich 1988; Frieman et al. 1995; Caldwell, Dave & Steinhardt 1998; Kaloper & Sorbo 2006; Chiba, Dutta & Scherrer 2009), or models that modify general relativity (see e.g. Sahni & Habib 1998; Parker & Raval 1999; Boisseau et al. 2000; Dvali, Gabadadze & Porrati 2000; Freese & Lewis 2002; Capozziello, Cardone & Troisi 2005; Padmanabhan 2009; Kahya, Onemli & Woodard 2010; O'Callaghan, Gregory & Pourtsidou 2009). For recent reviews, see Maartens (2004), Copeland, Sami & Tsujikawa (2006), Ratra & Vogeley (2008), Ruiz-Lapuente (2007), Frieman, Turner & Huterer (2008), Caldwell & Kamionkowski (2009), Uzan (2009), Woodard (2009) and Wang (2010). Several ground-based and space-born experiments have been proposed to determine the nature of cosmic

★E-mail: wang@nhn.ou.edu

acceleration through tight control of systematic effects and high statistical precision using multiple techniques.

A galaxy redshift survey in the near-infrared (IR) from space provides a powerful probe of dark energy and gravity, and has four key advantages over ground-based surveys:

(i) the ability to easily measure redshifts for galaxies at $z > 1$, especially in the so-called 'redshift desert' at $1.3 < z < 2$, given the low near-IR background,

(ii) the ability to measure redshifts for galaxies in both hemispheres in a single survey,

(iii) homogeneous data set and low level of systematics such as seeing and weather induced fluctuations in efficiency,

(iv) the speed of the survey (e.g. about 4 yr to cover $20\,000\,\mathrm{deg}^2$, see e.g. Laureijs et al. 2009).

Two proposed dark energy space missions, EUCLID[1] and JDEM,[2] are being considered by ESA and NASA/DOE, respectively.

Two main approaches have been considered so far for space-based massive spectroscopic surveys. The first is to use 'multislit' spectroscopy aimed at observing a pure magnitude-limited sample of galaxies selected in the near-IR (e.g. in the H band at $1.6\,\mu\mathrm{m}$) with a limiting magnitude appropriate to cover the desired redshift range. Examples of this approach are given by instruments where the efficient multislit capability is provided by microshutter arrays (MSA) (JEDI; Wang et al. 2004; Crotts et al. 2005; Cheng et al. 2006) or by digital micromirror devices (DMD) (SPACE; Cimatti et al. 2009). With the multislit approach, all galaxy types (from passive ellipticals to starbursts) are observed, provided that the targets are randomly selected from the magnitude-limited galaxy sample. The second approach is based on slitless spectroscopy (e.g. Glazebrook et al. 2005; Gehrels et al. 2009; Laureijs et al. 2009). Because of stronger sky background, the slitless approach is sensitive mostly to galaxies with emission lines [i.e. star-forming and active galactic nucleus (AGN) systems], and uses mainly Hα as a redshift tracer if the observations are done in the near-IR to cover the redshift range of interest for dark energy (e.g. $0.5 < z < 2$).

In this paper, we study the dark energy constraints expected from plausible galaxy redshift surveys from space. We will compare the various surveys using both the Dark Energy Task Force (DETF) figure-of-merit (FoM) for (w_0, w_a) (Albrecht et al. 2006), and more general dark energy FoMs motivated by the need to derive model-independent constraints on dark energy (Wang 2008a). In two accompanying papers, Majerotto et al. (in preparation) and Samushia et al. (2010), we will examine how space-based galaxy redshift surveys can test general relativity and are affected by cosmological model assumptions.

2 FORECASTING METHODOLOGY

Galaxy redshift surveys allow us to determine the time dependence of dark energy density by measuring the Hubble parameter $H(z)$ and the angular diameter distance $D_A(z) = r(z)/(1 + z)$ [where $r(z)$ is the comoving distance] as a function of redshift based on Baryon Acoustic Oscillation (BAO) measurements (Blake & Glazebrook 2003; Seo & Eisenstein 2003). BAO in the observed galaxy power spectrum provide a characteristic scale determined by the comoving sound horizon at the drag epoch (shortly after recombination), and

---

are theoretically well understood. The signature of the same physical process is clearly seen in the cosmic microwave background (CMB) anisotropy data (Komatsu et al. 2010), and these are often used to anchor low-redshift BAO to the epoch of last scattering. The observed BAO scale measures $sH(z)$ in the radial direction, and $D_A(z)/s$ in the transverse direction, where s is the sound horizon at the baryon drag epoch. Redshift-space distortions (RSD) produced by linear peculiar velocities (Kaiser 1987) have also been shown in recent years to represent a potentially powerful test of deviations from general relativity, the alternative way to explain the observed cosmic acceleration (Guzzo et al. 2008; Wang 2008b; Song & Percival 2009; Reyes et al. 2010). A large, deep redshift survey will be able to use RSD to measure the growth rate of density fluctuations $f_g(z_i)$ within the same redshift bins in which $H(z)$ will be estimated through BAO.

The observed galaxy power spectrum can be reconstructed assuming a reference cosmology, and can be approximated on large scales as (see e.g. Seo & Eisenstein 2003)

$$P_{\mathrm{obs}}(k_\perp^{\mathrm{ref}}, k_\parallel^{\mathrm{ref}}) = \frac{\left[D_A(z)^{\mathrm{ref}}\right]^2 H(z)}{[D_A(z)]^2 H(z)^{\mathrm{ref}}} b^2(1 + \beta\mu^2)^2$$
$$\times \left[\frac{G(z)}{G(0)}\right]^2 P_m(k)_{z=0} + P_{\mathrm{shot}}, \qquad (1)$$

where $b(z)$ is the bias factor between galaxy and matter density distributions, and $\beta(z)$ is the linear RSD parameter (Kaiser 1987). The growth factor $G(z)$ and the growth rate $f_g(z) = \beta b(z)$ are related via $f_g(z) = \mathrm{d}\ln G(z)/\mathrm{d}\ln a$, and $\mu = \boldsymbol{k} \cdot \hat{\boldsymbol{r}}/k$, with $\hat{\boldsymbol{r}}$ denoting the unit vector along the line of sight; $\boldsymbol{k}$ is the wavevector with $|\boldsymbol{k}| = k$. Hence $\mu^2 = k_\parallel^2/k^2 = k_\parallel^2/(k_\perp^2 + k_\parallel^2)$. The values in the reference cosmology are denoted by the superscript 'ref', while those in the true cosmology have no superscript. Note that

$$k_\perp^{\mathrm{ref}} = k_\perp \frac{D_A(z)}{D_A(z)^{\mathrm{ref}}}, \qquad k_\parallel^{\mathrm{ref}} = k_\parallel \frac{H(z)^{\mathrm{ref}}}{H(z)}. \qquad (2)$$

The shot noise P_{shot} is the unknown white shot noise that remains even after the conventional shot noise of inverse number density has been subtracted (Seo & Eisenstein 2003). These could arise from galaxy clustering bias even on large scales due to local bias (Seljak 2000). Equation (1) characterizes the dependence of the observed galaxy power spectrum on $H(z)$ and $D_A(z)$, as well as the sensitivity of a galaxy redshift survey to the RSD parameter β.

The measurement of $f_g(z)$ given $\beta(z)$ requires an additional measurement of the bias $b(z)$, which could be obtained from the galaxy bispectrum (Matarrese, Verde & Heavens 1997; Verde et al. 2002). However, this masks the fact that the redshift-space overdensity field has an additive contribution that is independent of bias: galaxies move as test particles in the matter flow, in a way that is independent of their internal properties. The normalization of the redshift-space effect depends on $f_g(z)\sigma_{8m}(z)$, and we rewrite equation (1) as

$$P_{\mathrm{obs}}(k_\perp^{\mathrm{ref}}, k_\parallel^{\mathrm{ref}}) = \frac{\left[D_A(z)^{\mathrm{ref}}\right]^2 H(z)}{[D_A(z)]^2 H(z)^{\mathrm{ref}}} C_0(k)$$
$$\times \left[\sigma_{8g}(z) + f_g(z)\sigma_{8m}(z)\mu^2\right]^2 + P_{\mathrm{shot}}, \qquad (3)$$

where we have defined

$$\sigma_{8m}^2(z) \equiv \int_0^\infty \frac{\mathrm{d}k}{k} \Delta^2(k|z) \left[\frac{3 j_1(kr)}{kr}\right]^2, \qquad (4)$$

$$r = 8\,h^{-1}\,\mathrm{Mpc}, \qquad \Delta^2(k|z) \equiv \frac{k^3 P_m(k|z)}{2\pi^2}, \qquad (5)$$

$$C_0(k) \equiv \frac{P_m(k|z)}{\sigma_{8m}^2(z)} = \frac{P_m(k|z=0)}{\sigma_{8m}^2(z=0)}, \tag{6}$$

where $j_1(kr)$ is spherical Bessel function. Note that

$$\sigma_{8g}(z) = b(z)\sigma_{8m}(z). \tag{7}$$

We have assumed linear bias for simplicity.

To study the expected impact of future galaxy redshift surveys, we use the Fisher matrix formalism. In the limit where the length scale corresponding to the survey volume is much larger than the scale of any features in $P(k)$, we can assume that the likelihood function for the band powers of a galaxy redshift survey is Gaussian (Feldman, Kaiser & Peacock 1994). Then the Fisher matrix can be approximated as (Tegmark 1997)

$$F_{ij} = \int_{k_{min}}^{k_{max}} \frac{\partial \ln P(\boldsymbol{k})}{\partial p_i} \frac{\partial \ln P(\boldsymbol{k})}{\partial p_j} V_{eff}(\boldsymbol{k}) \frac{\mathrm{d}k^3}{2(2\pi)^3}, \tag{8}$$

where p_i are the parameters to be estimated from data, and the derivatives are evaluated at parameter values of the fiducial model. The effective volume of the survey

$$\begin{aligned}
V_{eff}(k, \mu) &= \int \mathrm{d}\boldsymbol{r}^3 \left[\frac{n(\boldsymbol{r})P(k, \mu)}{n(\boldsymbol{r})P(k, \mu) + 1} \right]^2 \\
&= \left[\frac{nP(k, \mu)}{nP(k, \mu) + 1} \right]^2 V_{survey},
\end{aligned} \tag{9}$$

where in the second equation, the comoving number density n is assumed to only depend on the redshift for simplicity. Note that the Fisher matrix F_{ij} is the inverse of the covariance matrix of the parameters p_i if the p_i are Gaussian distributed. Equation (8) propagates the measurement error in $\ln P(\boldsymbol{k})$ (which is proportional to $[V_{eff}(\boldsymbol{k})]^{-1/2}$) into measurement errors for the parameters p_i.

To minimize non-linear effects, we restrict wavenumbers to the quasi-linear regime. We take $k_{min} = 0$, and k_{max} is given by requiring that the variance of matter fluctuations in a sphere of radius R, $\sigma^2(R) = 0.25$, for $R = \pi/(2k_{max})$. This gives $k_{max} \simeq 0.1\,h\,\mathrm{Mpc}^{-1}$ at $z = 0$, and $k_{max} \simeq 0.2\,h\,\mathrm{Mpc}^{-1}$ at $z = 1$, well within the quasi-linear regime. In addition, we impose a uniform upper limit of $k_{max} \leq 0.2\,h\,\mathrm{Mpc}^{-1}$ (i.e. $k_{max} = 0.2\,h\,\mathrm{Mpc}^{-1}$ at $z > 1$), to ensure that we are only considering the conservative linear regime essentially unaffected by non-linear effects.

The observed galaxy power spectrum in a given redshift shell centred at redshift z_i can be described by a set of parameters, $\{H(z_i), D_A(z_i), f_g(z_i)\sigma_{8m}(z_i), \sigma_{8g}(z_i), P_{shot}^i, \omega_m, \omega_b, n_s, h\}$, where $\omega_m = \Omega_m h^2 \propto \rho_m(z=0)$ (matter density today), $\omega_b = \Omega_b h^2 \propto \rho_b(z=0)$ (baryon density today), n_s is the power-law index of the primordial matter power spectrum and h is the dimensionless Hubble constant. Note that $P_m(k) \propto k^{n_s} T^2(k)$, with the matter transfer function $T(k)$ only depending on ω_m and ω_b (Eisenstein & Hu 1998),[3] if k were in units of Mpc^{-1}, and if the dark energy dependence of $T(k)$ can be neglected.

We marginalize over $\{\sigma_{8g}(z_i), P_{shot}^i\}$ in each redshift slice, and project $\{H(z_i), D_A(z_i), f_g(z_i)\sigma_{8m}(z_i), \omega_m, \omega_b, n_s, h\}$ into a final set of cosmological parameters (Wang 2006). We refer to this as the 'full $P(k)$ method, with growth information included', in which the growth information is included assuming that general relativity is valid. For more conservative dark energy constraints, we do not assume general relativity, and marginalize over $\{f_g(z_i)\sigma_{8m}(z_i)\}$ from each redshift slice (in addition to $\{\sigma_{8g}(z_i), P_{shot}^i\}$), and only project $\{H(z_i), D_A(z_i), \omega_m, \omega_b, n_s, h\}$ into the final set of cosmological

parameters. We refer to this as the 'full $P(k)$ method, marginalized over growth information'. The details of our implementation can be found in Wang (2006, 2008a). For an ultraconservative approach, we can marginalize over the cosmological parameters that describe the shape of the power spectrum, $\{\omega_m, \omega_b, n_s, h\}$, and only project $\{H(z_i), D_A(z_i)\}$ or $\{H(z_i), D_A(z_i), f_g(z_i)\sigma_{8m}(z_i)\}$ into the final set of cosmological parameters. We refer to this as the '$P(k)$-marginalized-over-shape' method. To change from one set of parameters to another, we use (Wang 2006)

$$F_{\alpha\beta} = \sum_{ij} \frac{\partial p_i}{\partial q_\alpha} F_{ij} \frac{\partial p_j}{\partial q_\beta}, \tag{10}$$

where $F_{\alpha\beta}$ is the Fisher matrix for a set of parameters $\boldsymbol{p}$, and F_{ij} is the Fisher matrix for a set of equivalent parameters $\boldsymbol{q}$.

Measurements of the growth rate $f_g(z)$ and the BAO are correlated and need to be considered simultaneously (Ballinger, Peacock & Heavens 1996; Simpson & Peacock 2010). Note that the BAO only approach from Seo & Eisenstein (2007) is similar to our '$P(k)$-marginalize-over-shape' approach, but we adopt a more general procedure that includes correlations between $\{H(z_i), D_A(z_i)\}$ and $\{f_g(z_i)\sigma_{8m}(z_i)\}$. Similarly, our approach is more general than that of White, Song & Percival (2009), who made predictions for RSD constraints in a way that does not take into account simultaneous BAO measurements.

We derive dark energy constraints with and without Planck priors. The Planck priors are included as discussed in Appendix B. We derive dark energy constraints with and without Planck priors, whose calculation is discussed in Appendix B. Given that Planck is already operating successfully, and the full Planck data will be available when a space-based galaxy survey is conducted (estimated to be around 2017), results including Planck priors are the most interesting for cosmological constraints. We have included results without Planck priors in order to show the level of the dependency on additional data, and to enable the reader to reproduce our results.

3 RELATIVE IMPORTANCE OF THE BASIC SURVEY PARAMETERS

Assuming the widely used linear dark energy equation of state (Chevallier & Polarski 2001; Linder 2003),

$$w_X(z) = w_0 + (1-a)w_a, \tag{11}$$

we now study the dependence of the DETF FoM for (w_0, w_a) on the basic survey parameters: redshift accuracy, minimum redshift of the survey and the survey area. We assume the fiducial cosmological model adopted in the Euclid Assessment Study Report (Laureijs et al. 2009): $\Omega_m = 0.25$, $\Omega_\Lambda = 0.75$, $h = 0.7$, $\sigma_8 = 0.80$, $\Omega_b = 0.0445$, $w_0 = -0.95$, $w_a = 0$, $n_s = 1$.

We assume a baseline survey of Hα emission line galaxies, based on slitless spectroscopy of the sky. The empirical redshift distribution of Hα emission line galaxies derived by Geach et al. (2010) from observed Hα luminosity functions was adopted along with the bias function derived by Orsi et al. (2010) using a galaxy formation simulation.

Predictions for the redshift distribution of Hα emitters are based on a simple model of the evolution of the observed Hα luminosity function since $z \sim 2$ (see Geach et al. 2010 for full details). Briefly, the model enforces a fixed space density over cosmic time, but allows $L^\star$ to increase with $(1+z)^Q$ evolution out to $z = 1.3$ before plateauing at $z > 1.3$. The exponent Q is determined by fitting the evolution of observed $L^\star$ derived by different workers using similarly selected Hα emitter samples over $0 < z < 1.3$. The 1σ

---

[3] The effect of massive neutrinos will be considered elsewhere.

uncertainty is determined by both the uncertainty of the observed $L^\star$ parameters and the redshift coverage windows of the various $H\alpha$ surveys employed. Combined with an uncertainty on the space density normalization, we are able to estimate the typical error in dN/dz at a given limiting flux. Note that this does not include the uncertainty in the shape of the faint-end slope of the luminosity function, which is fixed at $\alpha = -1.35$ in the model. However, at the flux limits likely to be practical to future dark energy (galaxy redshift) surveys, galaxy counts contributed by $L \ll L^\star$ galaxies will be negligible, and at $f_{H\alpha} > 10^{-16}\,\mathrm{erg\,s^{-1}\,cm^{-2}}$ this simple model can successfully reproduce the observed number counts of $H\alpha$ emitters over the main redshift range pertinent to future dark energy (galaxy redshift) surveys.

Orsi et al. (2010) present predictions for the abundance and clustering of $H\alpha$ emitters using two different versions of their galaxy formation model. The two models contain many elements in common, but have important differences in their treatment of the formation of massive galaxies. One model invokes a superwind ejection of baryons to suppress the gas cooling rate in massive haloes, whereas the other model uses the energy released from accretion on to a central supermassive black hole. Orsi et al. show that the predicted bias of $H\alpha$ selected galaxies does not vary significantly between these models (the upper panels of their fig. 11) and is therefore a robust prediction.

Note that we consider the redshift success rates $e = 0.35, 0.5, 0.7$ in all our results, thus effectively varying the redshift completeness over the entire plausible range. The uncertainties in the redshift distribution and bias function of $H\alpha$ emission line galaxies are subdominant compared to the uncertainty in the redshift success rate e, which in turn depends on the mission implementation and survey strategy.

We present most of our results in terms of the FoM for (w_0, w_a), the conventional FoM for comparing dark energy surveys proposed by the DETF (Albrecht et al. 2006). Fitting formulae are provided for $P(k)$ including growth information (denoted '$\mathrm{FoM}_{P(k)f_g}$'), and when growth information is marginalized over ('$\mathrm{FoM}_{P(k)}$'). The effect of extending the FoM definition is considered in Section 3.7.

To include the ongoing Sloan Digital Sky Survey III (SDSS-III) Baryon Oscillation Spectroscopic Survey (BOSS)[4] of luminous red galaxies (LRG) in our forecasts, we assume that the LRG redshifts are measured over $0.1 < z < 0.7$, with standard deviation $\sigma_z/(1 + z) = 0.001$, for a galaxy population with a fixed number density of $n = 3 \times 10^{-4}\,h^3\,\mathrm{Mpc^{-3}}$, and a fixed linear bias of $b = 1.7$, over a survey area of $10\,000\,(\deg)^2$.

3.1 Dependence on area

The FoM of (w_0, w_a) for a survey is linearly dependent on the effective survey volume V_{eff} (see equations 8 and 16), thus proportional to the survey area for a fixed redshift range. Fig. 1 shows the FoM for (w_0, w_a) for a slitless galaxy redshift survey as functions of the survey area. We find that the dependence on survey area, with or without Planck priors, is well approximated by

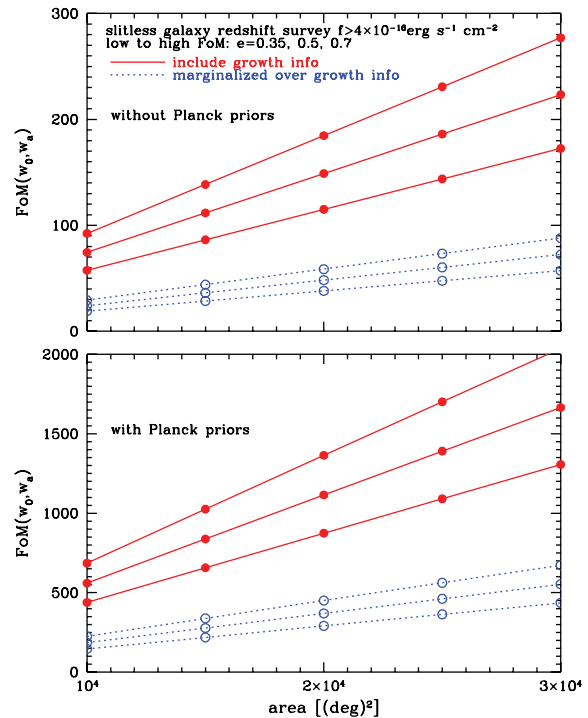$$\mathrm{FoM} \propto [\mathrm{area}]. \tag{12}$$

Figure 1. The FoM for (w_0, w_a) for a slitless galaxy redshift survey as a function of the survey area. We have assumed a survey of galaxies to a $H\alpha$ flux limit of $4 \times 10^{-16}\,\mathrm{erg\,s^{-1}\,cm^{-2}}$, with redshift success rates of $e = 0.35, 0.5, 0.7$ to an accuracy of $\sigma_z/(1 + z) = 0.001$, over a redshift range of $0.5 < z < 2.1$.

3.2 Dependence on redshift accuracy

The left-hand panels of Fig. 2 show the DETF FoM for (w_0, w_a) for a slitless galaxy redshift survey with flux limit of $4 \times 10^{-16}\,\mathrm{erg\,s^{-1}\,cm^{-1}}$, a survey area of $20\,000\,\deg^2$, and redshift success rates $e = 0.35, 0.5, 0.7$, respectively, as functions of redshift accuracy (for $0.5 \leq z \leq 2.1$). Appendix A1 gives the fitting formulae for the dependence of the FoM on the redshift accuracy for the various cases shown in the left-hand panel of Fig. 2.

The FoM increases rapidly as σ_z decreases for $\sigma_z/(1 + z) \leq 0.001$, but the rate of increase slows down beyond this limit (see left-hand panel of Fig. 2). There is a minimum redshift accuracy of $\sigma_z/(1 + z) \simeq 0.001$ that is important to achieve, but further accuracy is not important if the cost is high.

We have assumed that 35, 50 and 70 per cent (corresponding to redshift success rates of $e = 0.35, 0.5$ and 0.7) of objects have a correctly recovered redshift (with a redshift uncertainty $\sigma_z/(1 + z)$), and that there is no contaminating fraction. Performance simulations made for the EUCLID mission show that redshift uncertainties are randomly distributed. Given the objects' cross-contamination and the high background signal present in slitless observation, the redshift measurement is much more difficult with respect to the multislit case. To address this issue, a custom algorithm has been developed by Franzetti et al. (in preparation), which is strongly linked to the detection of the $H\alpha$ line within the observational window. This algorithm selects high-quality redshifts and makes line misidentification very rare, and results in randomly distributed redshift failures (Franzetti et al., in preparation).
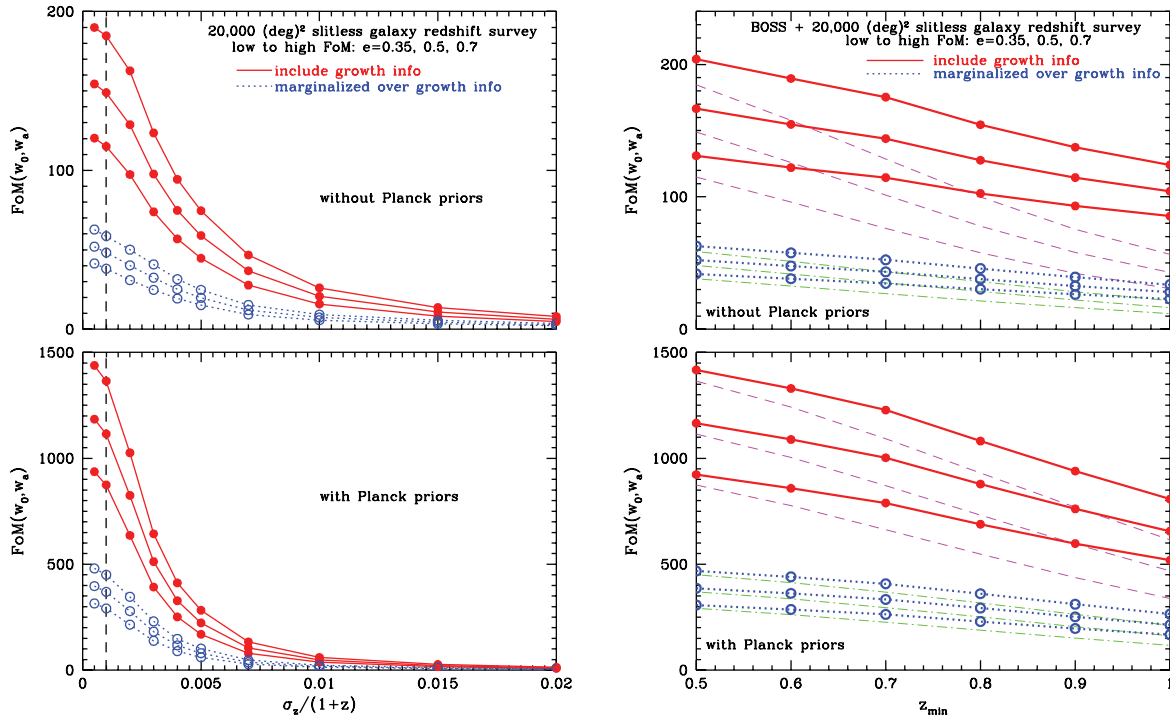
Figure 2. The FoM for (w_0, w_a) for a slitless galaxy redshift survey as functions of the redshift accuracy (left-hand panels) and the minimum redshift (right-hand panels) of the survey. We have assumed an Hα flux limit of 4×10^{-16} erg s^{-1} cm^{-2}, $z_{max} = 2.1$, a survey area of 20 000 (deg)^2, and redshift success rate $e = 0.35, 0.5, 0.7$, respectively. For the left-hand panels, we have assumed $z_{min} = 0.5$, and indicated our default assumption $\sigma_z/(1 + z) = 0.001$, assumed in the right-hand panel, with vertical dashed lines. The solid and dotted lines in each panel are the FoM for (w_0, w_a) with growth information included and marginalized over, respectively. Note that the right-hand panels include BOSS data at $z \leq 0.5$; the slitless redshift survey only FoMs are represented by the dashed and dot–dashed curves. The data points in the plots represent individual FoM calculations.

3.3 Dependence on redshift range

As discussed in Section 1, one of the primary advantages of a space-based survey is the ability to measure redshifts out to $z \simeq 2$. We therefore only consider changes to the minimum redshift limit of the sample. Although there will always be a tail to low redshift, we assume here that only redshifts greater than this minimum are used to constrain DE models. The right-hand panels in Fig. 2 show the FoM for (w_0, w_a) as a function of the minimum redshift of galaxies within the slitless survey assuming $z_{max} = 2.1$. The dashed and dot–dashed curves are with growth information included and marginalized over, respectively. The solid and dotted curves are similar to the dashed and dot–dashed curves, but include BOSS data for $z \leq z_{min}$. Appendix A2 gives the fitting formulae for the dependence of the FoM on the minimum redshift for the various cases shown in the right-hand panel of Fig. 2.

The low-redshift data have a strong effect on the DETF FoM, and the inclusion of BOSS becomes increasingly important as the minimum redshift of the slitless galaxy redshift survey is increased beyond $z = 0.7$, the maximum redshift covered by BOSS. It is clear that, purely based on the DETF FoM, it would be optimal to observe galaxies at lower redshifts. The bias of the DETF FoM to low redshifts has been discussed many previous times (e.g. Albrecht et al. 2009), and ignores the power of a space-based survey, as discussed in Section 1. This is a situation where it is obviously important to consider practical and instrumental issues, as well as a comparison with what can be achieved from the ground.

The redshift range of the survey of galaxies selected using a given method is usually fixed and derived from instrumentation. For example, for Hα flux selected galaxies observed from space,

a wavelength range between 1 and 2 µm driven by technical considerations, naturally imposes a redshift range $0.52 < z < 2.05$ in which Hα will be visible (Laureijs et al. 2009). The right-hand panel of Fig. 2 shows that, given this optimization method, it is better to choose the smallest minimum redshift allowed by the instrumentation, even when it overlaps with a ground-based survey.

Other arguments that should be considered for the optimal choice of the redshift range are (i) the capability to overlap (at least partly) with other complementary surveys which sample galaxies with a different biasing factor (e.g. BOSS/BigBOSS sampling luminous red galaxies at $0.1 < z < 1$ + EUCLID-like sampling star-forming galaxies at $0.5 < z < 2$), (ii) the maximization of the redshift range in order to have the largest leverage to constrain the potential evolution of the dark energy density. The importance of these considerations is demonstrated in Section 3.8.

3.4 Dependence on flux limit

We consider surveys with flux limits of 1, 2, 3, 4 and 5 $\times$ 10^{-16} erg s^{-1} cm^{-2}, and redshift success rates (the percentages of galaxies for which the measured redshifts have the specified redshift accuracy σ_z) of $e = 0.35, 0.5, 0.7$. Note that for simplicity, we have assumed the redshift success rates are constant with redshift. Clearly, a realistic success rate in measuring redshifts from a slitless survey will depend on Hα flux and redshifts. Ongoing simulations, however, show that the overall trends and relative FoMs discussed here are not significantly altered (Garilli et al., private communication).

The left-hand panel of Fig. 3 shows the effect of changing the Hα flux limit to a slitless survey (without adding Planck priors),
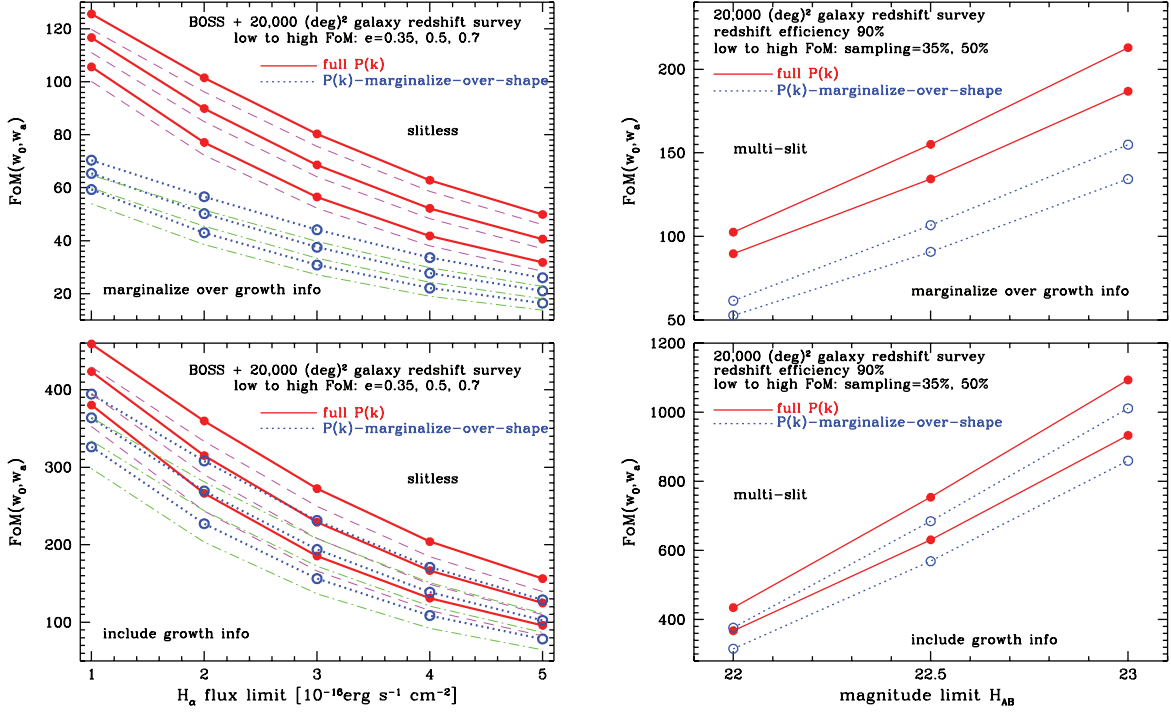
Figure 3. The FoM for (w_0, w_a) for a slitless galaxy redshift survey (left) as functions of the Hα flux limit, and a multislit galaxy redshift survey (right) as functions of the H-band magnitude limit of the survey. We have assumed $\sigma_z/(1 + z) = 0.001$, and a survey area of $20\,000\,(\text{deg})^2$. For the slitless survey, we have assumed $0.5 < z < 2.1$, redshift success rate $e = 0.35, 0.5, 0.7$, respectively. For the multislit survey, we have assumed a redshift efficiency of 90 per cent, and a redshift sampling rate of 35 and 50 per cent, respectively. The solid and dotted lines in each panel are the FoM for (w_0, w_a) with growth information included and marginalized over, respectively. Note that the left-hand panel includes BOSS data at $z \leq 0.5$; the slitless redshift survey only FoMs are represented by the dashed and dot–dashed curves. Planck priors are not included.

assuming that the data are taken to a uniform depth. Appendix A3 gives the fitting formulae for the dependence of the FoM on the Hα flux limit for the various cases shown in the left-hand panel of Fig. 3, with and without Planck priors.

As we saw previously for the minimum redshift, the addition of BOSS data to a slitless galaxy redshift survey makes a notable improvement on the FoM for (w_0, w_a) covering the low-redshift range where $H(z)$ is more sensitive to dark energy if dark energy evolution is small. Our fiducial model assumes a constant dark energy equation of state $w = -0.95$, which implies a very weak evolution in the dark energy density function $X(z)$.

3.5 Dependence on spectroscopic method

We compare against a H-band magnitude limited survey of randomly sampled galaxies enabled by multislit spectroscopy, e.g. by means of programmable DMD (SPACE; Cimatti et al. 2009), or MSA (JEDI; Wang et al. 2004; Crotts et al. 2005; Cheng et al. 2006). To predict galaxy densities for such surveys we use the empirical galaxy redshift distribution compiled by Zamorani et al. from existing data (see Laureijs et al. 2009), and we use predictions of galaxy bias from galaxy formation simulations (Orsi et al. 2010). Our adopted H-band selected galaxy redshift distribution has been compiled from observations in the COSMOS survey and the *Hubble Ultra-Deep Field*, where excellent photometric redshifts are available. The bias function for Hα flux and H-band magnitude selected galaxies increase with redshift, with the former being less strongly biased than the latter (Orsi et al. 2010). The H band traces massive structures (similar to selecting galaxies in the K band), which makes them strongly biased. Star-forming galaxies (which are se-

lected by Hα flux), on the other hand, appear to avoid the cores of clusters and populate the filaments of the dark matter structure, making them less biased than H-band galaxies (Orsi et al. 2010). We consider multislit surveys with limiting magnitudes of $H_{\text{AB}} = 22, 22.5$ and 23, a redshift success rate of 90 per cent, and sampling rates of 35 and 50 per cent.

Fig. 3 compares FoM for (w_0, w_a) for slitless and multislit galaxy redshift surveys (without adding Planck priors). BOSS data are not added to the multislit galaxy redshift surveys, which have redshift ranges that extend to $z \sim 0.1$ (Cimatti et al. 2009; Laureijs et al. 2009). Appendix A4 gives the fitting formulae for the dependence on the H-band magnitude limit for the various cases shown in the right-hand panel of Fig. 3, with and without Planck priors.

The total number of galaxies with redshifts (measured with $\sigma_z/(1 + z) \leq 0.001$) from a slitless survey is well approximated by

$$\frac{N_{\text{gal}}}{10^6} = 276.74 \, \frac{[\text{area}]}{20\,000} \, \frac{e}{0.5} \, \left(\bar{f}\right)^{-0.9(\bar{f})^{0.14}}, \tag{13}$$

where $\bar{f} \equiv f/[10^{-16}\,\text{erg s}^{-1}\,\text{cm}^{-2}]$.

The total number of galaxies with redshifts (measured with $\sigma_z/(1 + z) \leq 0.001$) from a multislit survey is well approximated by

$$\frac{N_{\text{gal}}}{10^6} = \left[192.21 + 197.03\,(H_{\text{AB}} - 22)^{1.3}\right] \frac{[\text{area}]}{20\,000} \frac{e}{0.9 \times 0.35}. \tag{14}$$

Multislit surveys give significantly larger FoM than slitless surveys, because they allow the accurate redshift measurement for a greater number of galaxies (and these galaxies are more biased tracers of large-scale structure than star-forming galaxies), and over a greater redshift range (extending to $z \sim 0.1$). However, they have
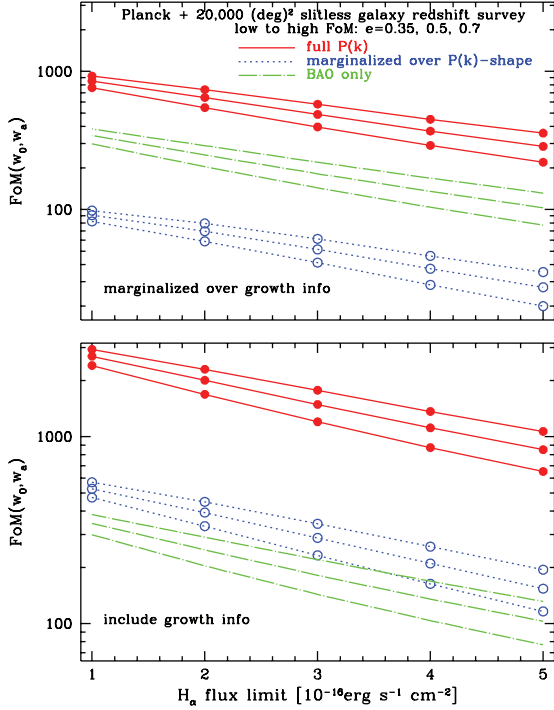
Figure 4. The FoM for (w_0, w_a) for a slitless galaxy redshift survey combined with Planck priors, as functions of the Hα flux limit, for three different forecast methods. We have assumed $0.5 < z < 2.1$, $\sigma_z/(1 + z) = 0.001$, a survey area of $20\,000\,(\text{deg})^2$, and redshift success rate $e = 0.35, 0.5, 0.7$ (curves from bottom to top), respectively.

substantially stronger requirements in instrumentation and mission implementation (Cimatti et al. 2009).

3.6 Dependence on clustering information used

Fig. 4 shows the FoM for (w_0, w_a) for a slitless galaxy redshift survey combined with Planck priors, as functions of the Hα flux limit, for three different levels of clustering information used: the full $P(k)$ (solid lines), $P(k)$-marginalized-over-shape (dotted lines) and BAO only (dot–dashed lines). For the full $P(k)$ and $P(k)$-marginalize-over-shape methods, the top panel of Fig. 4 shows the FoM obtained after marginalization over growth information, while the lower panel shows the FoM obtained including the growth information. For the BAO only method, the FoMs are the same in the upper and lower panels, and obtained without adding the growth information, since the inclusion of growth information is precluded by construction in this method: in the BAO only method, the power spectrum with baryonic features is approximated by (Seo & Eisenstein 2007)

$$P_b(k, \mu|z) \propto \frac{\sin(x)}{x}, \qquad x \equiv \left(k_\perp^2 s_\perp^2 + k_\parallel^2 s_\parallel^2\right)^{1/2}. \qquad (15)$$

The only parameters estimated in this method are the BAO scales in the transverse and radial directions, $s_\perp$ and $s_\parallel$. To include growth information, the Fisher matrix needs to be expanded to include $f_g(z)\sigma_{8m}(z)$ and $\sigma_{8g}(z)$ for each redshift slice. However, RSD affect the amplitude of the full power spectrum, without the damping factor of $\sin(x)/x$ in the BAO approximation of equation (15). While this damping factor does not affect the predictions of $s_\perp$ or $s_\parallel$ (the derivative of $\sin(x)/x$ by $s_\perp$ or $s_\parallel$ is independent of k to leading order), it would incorrectly affect predictions of $f_g(z)\sigma_{8m}(z)$ and $\sigma_{8g}(z)$ if this formula was naively applied to predict growth constraints.

However, it is possible to envisage a scenario where BAO are used to provide geometrical constraints, while a coupled measurement of RSD is used based on the full power spectrum.

When the growth information is marginalized over, the constraints from the BAO only method are much stronger than those from the $P(k)$-marginalize-over-shape method, with the addition of Planck priors (see upper panel of Fig. 4). This is because the BAO only method implicitly assumes that the shape of BAO (i.e. $P(k)$) are fixed by CMB data, while the $P(k)$-marginalize-over-shape method allows the $P(k)$ shape to vary and then discards the information of how cosmological constraints are coupled to $P(k)$ shape. When growth information is included, the information loss due to the marginalization over the shape of $P(k)$ is reduced, allowing a higher gain in FoM when Planck priors are added (see lower panel of Fig. 4).

Fig. 4 shows that both the $P(k)$-marginalize-over-shape method and the BAO only method give conservative estimates of dark energy constraints. Compared to the BAO only method, the $P(k)$-marginalize-over-shape method (including growth information) has the advantage of allowing the consistent inclusion of growth information in that, if we assume we can use the power spectrum shape and amplitude to obtain RSD information, then it is sensible to also assume we can at least partially use it as a standard ruler.

3.7 Dependence on DE parametrization

We now consider the effect of changing to the generalized DE parametrization (Wang 2008a), with the dimensionless dark energy density $X(z) \equiv \rho_X(z)/\rho_X(z = 0)$ given by interpolating its value at $z_i, i = 1, 2, \ldots, N$. We consider $z_i = i \times 2.0/N$ ($i = 1, 2, \ldots, N$) with $N = 3$, i.e., $(X_{0.67}, X_{1.33}, X_{2.0})$. We use linear interpolation here since it gives the most conservative estimates. Using this parametrization, we can define a dark energy FoM (Wang 2008a):

$$\text{FoM}(p_1, p_2, p_3, \ldots) = \frac{1}{\sqrt{\det \text{Cov}(p_1, p_2, p_3, \ldots)}}, \qquad (16)$$

where $\{p_i\}$ are the chosen set of dark energy parameters. This definition has the advantage of being easy to calculate for either real or simulated data, and applicable to any set of dark energy parameters. If the likelihood surfaces for all the parameters are Gaussian, this FoM is proportional to the inverse of the N-dimensional volume enclosed by the 68 per cent confidence level (C.L.) contours of the parameters $(p_1, p_2, p_3, \ldots)$. For $N = 2$ and $(p_1, p_2) = (w_0, w_a)$, equation (16) reduces to the FoM used by the DETF (Albrecht et al. 2006), FoM(w_0, w_a).[5]

We now show the impact of parametrizing dark energy density function, $X(z) \equiv \rho_X(z)/\rho_X(0)$, using its value at equally spaced redshifts, $(X(z_1), X(z_2), \ldots, X(z_N))$. Fig. 5 shows the FoM (without Planck priors) for $(X_{0.67}, X_{1.33}, X_{2.0})$ for slitless (left-hand panels) and multislit (right-hand panels) galaxy redshift surveys, as functions of the Hα flux limit for the slitless survey, and of the H-band magnitude limit for the multislit survey. Note that the subscripts on X indicate the redshift values.

We find that the addition of BOSS data to a slitless galaxy redshift survey does *not* make a notable improvement on the FoM for

---

[5] The DETF defined the dark energy FoM to be the inverse of the area enclosed by the 95 per cent C.L. contour of (w_0, w_a), which is equal to the FoM given by equation (16) multiplied by a constant factor of $1/(6.17\pi)$. However, this constant factor is always omitted, even in the tables from the DETF report (Albrecht et al. 2006). Thus for all practical purposes, equation (16) is the same as the DETF FoM for (w_0, w_a).
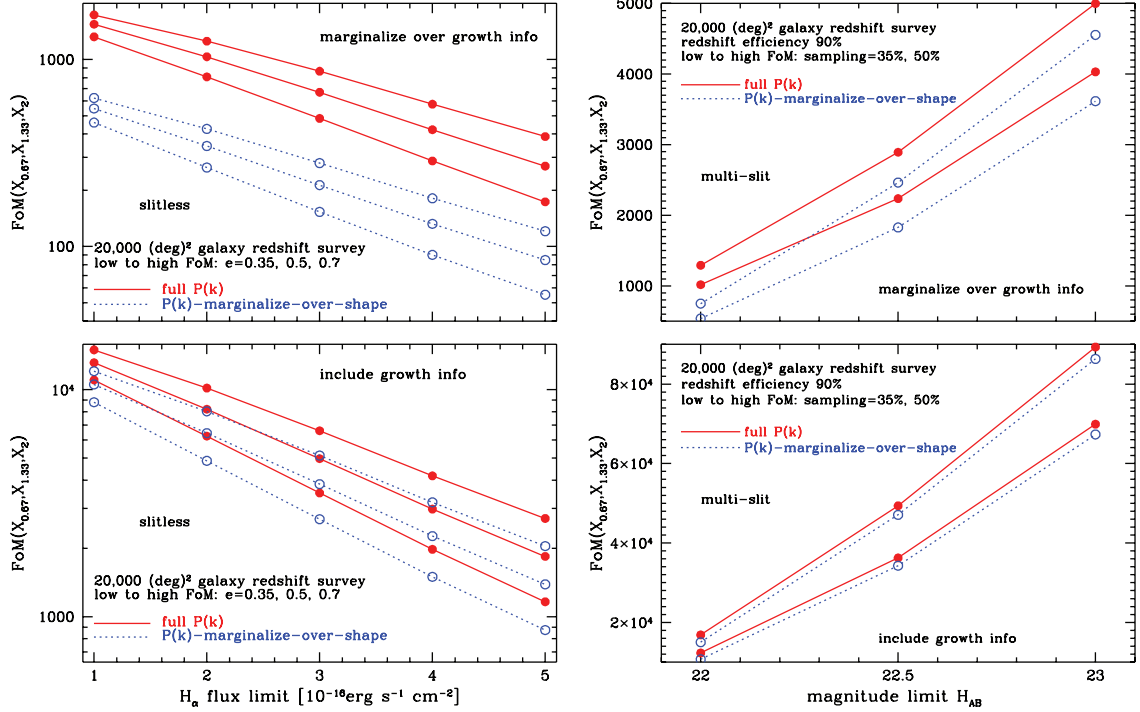
Figure 5. The FoM for $\{X_{0.67}, X_{1.33}, X_{2.0}\}$ for a slitless galaxy redshift survey (left) as functions of the Hα flux limit, and for a multislit galaxy redshift survey (right) as functions of the H-band magnitude limit of the survey. We have assumed a survey area of $20\,000\,(\text{deg})^2$ and $\sigma_z/(1 + z) = 0.001$. For the slitless survey, we have assumed $0.5 < z < 2.1$, and redshift success rate $e = 0.35, 0.5, 0.7$, respectively. For the multislit survey, we have assumed a redshift efficiency of 90 per cent, and a redshift sampling rate of 35 and 50 per cent, respectively.

$(X_{0.67}, X_{1.33}, X_{2.0})$, unlike the DETF FoM (see Fig. 3). Adding additional parameters to parametrize $X(z)$ gives qualitatively similar results. This difference arises because fits to w_0 and w_a tend to give strongly correlated results, decreasing the redshift range over which we are sensitive to DE changes. Fits using the parameter set $(X_{0.67}, X_{1.33}, X_{2.0})$ tend to be less correlated, increasing the sensitivity to the behaviour of dark energy at the highest redshifts at which dark energy is important. Note that multislit surveys would allow us to probe dark energy density at $z > 2$ by adding $X_{2.5}$ and $X_{3.0}$ to our parameter set.

The FoM for $(X_{0.67}, X_{1.33}, X_{2.0})$ is large, mainly because it involve an extra parameter compared to (w_0, w_a). For parameters $(p_1, p_2, p_3, \ldots)$ that are well constrained by a survey, FoM$(p_1, p_2, p_3, \ldots)$ roughly scales as $1/[\sigma(p_1)\sigma(p_2)\sigma(p_3)\ldots]$.

3.8 Comparison with ground-based surveys

Tables 1 and 2 compare the dark energy constraints from fiducial space-based slitless and multislit surveys to that of a generic ground-based survey. The space-based slitless and multislit surveys are those considered by EUCLID (Laureijs et al. 2009). The fiducial slitless survey is assumed to have an Hα flux limit of $4\times 10^{-16}\,\text{erg}\,\text{s}^{-1}\,\text{cm}^{-2}$ (at 7σ), a redshift range of $0.5 < z < 2.1$, $\sigma_z/(1 + z) = 0.001$, redshift efficiency $e = 0.5$ and a survey area of $20\,000\,(\text{deg})^2$. The fiducial multislit survey is assumed to have a H-band magnitude limit of $H_{AB} = 22$ (at 5σ), redshift success rate of 90 per cent, sampling rate of 35 per cent, $\sigma_z/(1 + z) = 0.001$ and a survey area of $20\,000\,(\text{deg})^2$.

The generic ground-based survey has a redshift range of $0.1 < z < 1.4$, $\sigma_z/(1 + z) = 0.001$, a fixed galaxy number density of $n =$

$3 \times 10^{-4}\,h^3\,\text{Mpc}^{-3}$, a fixed linear bias of $b = 1.7$,[6] and a survey area of $10\,000\,(\text{deg})^2$. Such a galaxy redshift survey can be conducted using a single ground-based telescope, and select galaxies based on standard optical colours.[7] This essentially extends the BOSS survey of LRGs from $z = 0.7$ to 1.4. If more than a single telescope is available for a ground-based survey, the survey area can be significantly larger than $10\,000\,(\text{deg})^2$ (see e.g. Schlegel et al. 2009), then the FoM for dark energy will be increased by the same factor as it scales with the survey area. While it is possible for ground-based surveys to achieve similar area coverage as a satellite mission, this would either require two instruments or a move after completing one survey, causing the experiment to have a very long duration.

As a reference, the DETF found that the Stage II projects (current and ongoing surveys) give FoM$(w_0, w_a) \sim 50$ when combined with Planck priors (Albrecht et al. 2006). Current data give FoM$(w_0, w_a) \sim 10$–20 (Wang 2009). Clearly, a space-based galaxy redshift survey (together with Planck data) can potentially increase the FoM(w_0, w_a) by a factor of ~ 100 compared to current data, and more than a factor of 10 compared to Stage II projects.

Note that the survey parameter assumptions adopted here for space- and ground-based surveys do *not* reflect the limits of such surveys, but are just fiducial cases generally considered feasible by

---

[6] The current best estimate for the low-z SDSS LRGs is $b = 1.7$ (Reid et al. 2010). Extending this assumption to higher redshift LRGs is conservative for passive evolution of LRGs. For emission line galaxies, however, $1 \lesssim b \lesssim 1.3$ for $0.7 \leq z \leq 1.4$ (Orsi et al. 2010).
[7] The proposed PAU project will measure the redshifts of red, early-type galaxies in the interval $0.1 < z < 0.9$, with $\sigma_z/(1 + z) < 0.003$ (achieved using 40 narrow filters and two broad filters), and cover $8000\,(\text{deg})^2$ (Benitez et al. 2009).

Table 1. The DETF FoM and 1σ marginalized errors for (w_0, w_a) for fiducial space-based slitless and multislit surveys, and a generic ground-based survey.

Method	dw_0	dw_a	dw_p	FoM (w_0, w_a)	dw_0	dw_a	dw_p	FoM (w_0, w_a)
	Fiducial	Slitless			+Planck			
$P(k)$	0.103	0.433	0.048	48.26	0.067	0.140	0.0193	369.58
$P(k)f_g$	0.072	0.274	0.024	148.93	0.023	0.061	0.0148	1114.91
	Fiducial	Multislit			+Planck			
$P(k)$	0.078	0.318	0.035	89.70	0.050	0.103	0.0169	576.44
$P(k)f_g$	0.049	0.182	0.015	367.51	0.017	0.044	0.0119	1907.60
	Fiducial	Ground			+Planck			
$P(k)$	0.182	0.830	0.111	10.82	0.156	0.360	0.0362	76.83
$P(k)f_g$	0.120	0.612	0.050	32.88	0.049	0.130	0.0305	253.28

Table 2. The FoM and 1σ marginalized errors for $(X_{0.67}, X_{1.33}, X_{2.0})$ for fiducial space-based slitless and multislit surveys, and a generic ground-based survey.

Method	$dX_{0.67}$	$dX_{1.33}$	$dX_{2.0}$	FoM $\{X_i\}$	$dX_{0.67}$	$dX_{1.33}$	$dX_{2.0}$	FoM $\{X_i\}$
	Fiducial	Slitless			+Planck			
$P(k)$	0.115	0.287	0.624	421.26	0.059	0.058	0.163	3487.41
$P(k)f_g$	0.055	0.164	0.389	2979.49	0.028	0.046	0.101	26 659.23
	Fiducial	Multislit			+Planck			
$P(k)$	0.080	0.187	0.422	1017.92	0.052	0.051	0.125	6657.24
$P(k)f_g$	0.032	0.082	0.201	12 300.00	0.024	0.038	0.081	59 674.89
	Fiducial	Ground			+Planck			
$P(k)$	0.232	0.600	6.011	3.46	0.106	0.174	4.703	27.92
$P(k)f_g$	0.132	0.400	2.596	31.14	0.049	0.099	1.703	246.15

the community. We find that while a sufficiently wide ground-based survey (requiring more than one telescope) could give a similar FoM for (w_0, w_a) compared with a conservative space-based slitless survey, it will not give competitive FoM for $(X_{0.67}, X_{1.33}, X_{2.0})$ (see Table 2).

It is important to recognize that both space and ground galaxy redshift surveys are required to obtain definitive measurement of dark energy using galaxy clustering. Ongoing ground-based surveys, BOSS and WiggleZ,[8] will enable us to test the methodology for extracting dark energy constraints from galaxy clustering data, and improve our understanding of systematic effects. Proposed ground-based surveys, such as BigBOSS (Schlegel et al. 2009) and HETDEX,[9] will be complementary to space-based surveys in using different tracer populations and redshift coverage.

There are other tracers of cosmic large-scale structure that can be observed from the ground, and are also highly complementary in probing dark energy to the space-based surveys discussed in this paper. For example, ground-based Lyα forest data can be used to study clustering of matter at $z = 2$ to 4 (Croft et al. 2002), and help constrain the early evolution of dark energy. Another example is the use of galaxy redshift surveys based on the radio HI emission line at 21 cm to probe dark energy. Galaxy redshift surveys made possible by the Square Kilometre Array (SKA) could use 21-cm emission to observe galaxies out to $z \sim 1.5$ (Abdalla, Blake & Rawlings 2010), but the time-scale for such experiments is longer than that of the currently proposed space-based surveys.

The overlap in redshift ranges of space- and ground-based surveys is critical for understanding systematic effects such as bias using

multiple tracers of cosmic large-scale structure (e.g. Hα-selected galaxies from a space-based survey, and LRGs from a ground-based survey). The use of multiple tracers of cosmic large-scale structure can ultimately increase the precision of dark energy measurements from galaxy redshift surveys (Seljak, Hamaus & Desjacques 2009).

4 SUMMARY

Recent studies (e.g. Cimatti et al. 2009) have shown that near-IR multislit spectroscopic surveys provide a very efficient approach for studying dark energy and would also provide data of sufficient quality for many other cosmological applications. Slitless spectroscopy can also be very efficient and competitive if some critical top level requirements are met such as the survey sky coverage, the redshift accuracy and the number of galaxies. In particular, the combination of space-based survey and ground-based survey should encompass the entire redshift range, $0 \lesssim z \lesssim 2$, in which dark energy becomes important. The ongoing ground-based survey that covers the widest area ($10\,000\,\mathrm{deg}^2$), BOSS, will span the redshift range of $0.1 < z < 0.7$. The redshift range of $0.5 \lesssim z \lesssim 2.1$ can be achieved by a space mission with near-IR 1–2 μm wavelength coverage targeting Hα emission-line galaxies (Cimatti et al. 2009); expanding this redshift range would increase the complexity of a space mission.

Our key findings from this paper are following.

(i) The redshift range of $0.5 \lesssim z \lesssim 2.1$ is appropriate, since it exploits the redshift range that is only easily accessible from space, extends to sufficiently low redshifts to allow both a vast 3D map of the Universe using a single tracer population, and overlapping with ground-based surveys such as BOSS and BigBOSS to enable

[8] http://wigglez.swin.edu.au/
[9] http://hetdex.org/

reliable modelling of systematic effects and increased statical precision.

(ii) For a given survey depth, the dark energy FoM for (w_0, w_a) increases linearly with the survey area. Thus it is optimal to cover the entire extragalactic sky ($\sim 30\,000\,\mathrm{deg}^2$). The actual sky coverage of a given space-based survey will be constrained by cost and mission duration. The sky coverage of $\geq 20\,000\,(\mathrm{deg})^2$ can give powerful dark energy constraints (see Fig. 1).

(iii) There is a trade-off between survey area and survey depth for a given mission implementation. Given the same total amount of exposure time, maximizing the survey area gives the largest dark energy FoM, compared to decreasing the survey area while increasing the survey depth. The depth of the survey and the efficiency of the redshift measurements are strongly constrained by the feasibility of the space mission instrumentation. We have assumed very conservative efficiencies for the redshift measurements (Franzetti et al., in preparation). Taking into consideration the need to simplify the mission implementation and reduce mission risks, a survey area of $20\,000\,(\mathrm{deg})^2$ is feasible for a slitless survey with an Hα flux limit of $4 \times 10^{-16}\,\mathrm{erg\,s^{-1}\,cm^{-2}}$, or a multislit survey with a H-band magnitude limit of $H_{AB} < 22$ (Cimatti et al. 2009; Laureijs et al. 2009).

(iv) A space-based galaxy redshift survey, optimized as discussed in this paper, has enormous power in constraining dark energy (see Figs 2–5 and Tables 1–2). The gain in dark energy FoM of an optimized space-based survey is most dramatic over ground-based surveys when dark energy density is allowed to be a free function parametrized by its values at equally spaced redshift values extending to $z = 2$ (thus allowing a model-independent measurement of dark energy) (see Table 2).

(v) The growth information from a galaxy redshift survey plays a critical role in boosting the dark energy FoM of the survey, assuming that general relativity is not modified. This is not surprising, since existing measurements of the growth rate $f_g(z)$ have been used in the past to help tighten dark energy constraints (see e.g. Knop et al. 2003; Wang & Mukherjee 2004). We find that when growth information from $P(k)$ is included in the analysis, we gain a factor of ~ 3 in the DETF dark energy FoM, compared to when the growth information is marginalized over. This is because the growth rate $f_g(z)$ is anticorrelated with $H(z)$.

(vi) We show that in order to consistently include the growth information, the full galaxy power spectrum $P(k)$ must be used (i.e. the '$P(k)$ method'). We can obtain conservative constraints if we marginalize over the cosmological parameters that determine the shape of $P(k)$ (see Fig. 4).

Probing dark energy using multiple techniques (galaxy clustering, weak lensing, supernovae), each with tight controls of systematic effects, will ultimately illuminate the nature of dark energy (Wang et al. 2004; Crotts et al. 2005; Cheng et al. 2006). A space-based galaxy redshift survey will play a key role in advancing our understanding of dark energy.

REFERENCES

Abdalla F. B., Blake C., Rawlings S., 2010, MNRAS, 401, 743
Albrecht A. et al., 2006, Report of the Dark Energy Task Force, preprint (astro-ph/0609591)
Albrecht A. et al., 2009, Findings of the Joint Dark Energy Mission Figure of Merit Science Working Group, preprint (arXiv:0901.0721)
Ballinger W. E., Peacock J. A., Heavens A. F., 1996, MNRAS, 282, 877
Benitez N. et al., 2009, ApJ, 691, 241
Blake C., Glazebrook K., 2003, ApJ, 594, 665
Boisseau B., Esposito-Farèse G., Polarski D., Starobinsky A. A., 2000, Phys. Rev. Lett., 85, 2236
Caldwell R. R., Kamionkowski M., 2009, Annu. Rev. Nuclear Part. Sci., 59, 397
Caldwell R., Dave R., Steinhardt P. J., 1998, Phys. Rev. Lett., 80, 1582
Capozziello S., Cardone V. F., Troisi A., 2005, Phys. Rev. D, 71, 043503
Cheng E. et al., 2006, Proc. SPIE, 6265, 626529
Chevallier M., Polarski D., 2001, Int. J. Modern Phys. D, 10, 213
Chiba T., Dutta S., Scherrer R. J., 2009, Phys. Rev. D, 80, 043517
Cimatti A. et al., 2009, Exp. Astron., 23, 39
Copeland E. J., Sami M., Tsujikawa S., 2006, Int. J. Modern Phys. D, 15, 1753
Croft R. A. C., Weinberg D. H., Bolte M., Burks S., Hernquist L., Katz N., Kirkman D., Tyler D., 2002, ApJ, 581, 20
Crotts A. et al., 2005, preprint (astro-ph/0507043)
Dvali G., Gabadadze G., Porrati M., 2000, Phys. Lett. B, 485, 208
Eisenstein D., Hu W., 1998, ApJ, 496, 605
Feldman H. A., Kaiser N., Peacock J. A., 1994, ApJ, 426, 23
Freese K., Lewis M., 2002, Phys. Lett. B, 540, 1
Freese K., Adams F. C., Frieman J. A., Mottola E., 1987, Nuclear Phys. B, 287, 797
Frieman J. A., Hill C. T., Stebbins A., Waga I., 1995, Phys. Rev. Lett., 75, 2077
Frieman J., Turner M., Huterer D., 2008, ARA&A, 46, 385
Geach J. E. et al., 2010, MNRAS, 402, 1330
Gehrels N. et al., 2009, Final Report of the Joint Dark Energy Mission Science Coordination Group, http://jdem.gsfc.nasa.gov/science/scg/
Glazebrook K., Baldry J., Moos W., Kruk J., McCandliss S., 2005, New Astron. Rev., 49, 374
Guzzo L. et al., 2008, Nat, 451, 541
Hu W., Sugiyama N., 1996, ApJ, 471, 542
Kahya E. O., Onemli V. K., Woodard R. P., 2010, Phys. Rev. D, 81, 023508
Kaiser N., 1987, MNRAS, 227, 1
Kaloper N., Sorbo L., 2006, J. Cosmology Astropart. Phys., 0604, 007
Knop R. A. et al., 2003, ApJ, 598, 102
Komatsu E. et al., 2010, preprint (arXiv:1001.4538)
Laureijs R. et al., 2009, Euclid Assessment Study Report for the ESA Cosmic Visions, preprint (arXiv:0912.0914)
Lewis A., Bridle S., 2002, Phys. Rev. D, 66, 103511
Lewis A., Challinor A., Lasenby A., 2000, ApJ, 538, 473
Linde A. D., 1987, in Hawking S. W., Israel W., eds, Three Hundred Years of Gravitation. Cambridge Univ. Press, Cambridge, p. 604
Linder E. V., 2003, Phys. Rev. Lett., 90, 091301
Maartens R., 2004, Living Rev. Relativ., 7, 7
Matarrese S., Verde L., Heavens A. F., 1997, MNRAS, 290, 651
Mukherjee P., Kunz M., Parkinson D., Wang Y., 2008, Phys. Rev. D, 78, 083529
O'Callaghan E., Gregory R., Pourtsidou A., 2009, J. Cosmology Astropart. Phys., 0909, 020
Orsi A., Baugh C. M., Lacey C. G., Cimatti A., Wang Y., Zamorani G., 2010, MNRAS, 405, 1006
Padmanabhan T., 2009, Advanced Sci. Lett., 2, 174
Pahud C., Liddle A. R., Mukherjee P., Parkinson D., 2006, Phys. Rev. D, 73, 123524

Parker L., Raval A., 1999, Phys. Rev. D, 60, 063512
Peebles P. J. E., Ratra B., 1988, ApJ, 325, L17
Perlmutter S. et al., 1999, ApJ, 517, 565
Ratra B., Vogeley M. S., 2008, PASP, 120, 235
Reid B. A. et al., 2010, MNRAS, 404, 60
Reyes R., Mandelbaum R., Seljak U., Baldauf T., Gunn J. E., Lombriser L.,
    Smith R. E., 2010, Nat, 464, 256
Riess A. G. et al., 1998, AJ, 116, 1009
Ruiz-Lapuente P., 2007, Classical Quantum Gravity, 24, 91
Sahni V., Habib S., 1998, Phys. Rev. Lett., 81, 1766
Samushia L. et al., 2010, preprint (arXiv:1006.0609)
Schlegel D. J. et al., 2009, arXiv:0904.0468
Seljak U., 2000, MNRAS, 318, 203
Seljak U., Hamaus N., Desjacques V., 2009, Phys. Rev. Lett., 103, 091303
Seo H., Eisenstein D. J., 2003, ApJ, 598, 720
Seo H., Eisenstein D. J., 2007, ApJ, 665, 14
Simpson F., Peacock J. A., 2010, Phys. Rev. D, 81, 043512
Song Y.-S., Percival W. J., 2009, J. Cosmology Astropart. Phys., 10, 004
Tegmark M., 1997, Phys. Rev. Lett., 79, 3806
Uzan J.-P., 2009, preprint (arXiv:0908.2243)
Verde L. et al., 2002, MNRAS, 335, 432
Wang Y., 2006, ApJ, 647, 1
Wang Y., 2008a, Phys. Rev. D, 77, 123525
Wang Y., 2008b, J. Cosmology Astropart. Phys., 05, 021
Wang Y., 2009, Phys. Rev. D, 80, 123525
Wang Y., 2010, Dark Energy. Wiley-VCH, Weinheim
Wang Y., Mukherjee P., 2004, ApJ, 606, 654
Wang Y., Mukherjee P., 2006, ApJ, 650, 1
Wang Y., Mukherjee P., 2007, Phys. Rev. D, 76, 103533
Wang Y., Tegmark M., 2004, Phys. Rev. Lett., 92, 241302
Wang Y. et al., 2004, BAAS, 36, 1560
Wetterich C., 1988, Nuclear Phys. B, 302, 668
White M., Song Y.-S., Percival W. J., 2009, MNRAS, 397, 1348
Woodard R. P., 2009, Rep. Progress Phys., 72, 126002

APPENDIX A: FITTING FORMULAE FOR DARK ENERGY FOM

The fitting formulae for dark energy FoM correspond to the figures in Section 3.

A1 Dependence of DETF FoM on the redshift accuracy

The fitting formulae of the dependence of the DETF FoM on the redshift accuracy presented here correspond to the curves in left-hand panels of Fig. 2. The dependence of the FoM for (w_0, w_a) on the redshift accuracy is well approximated by

$$
\mathrm{FoM}_{P(k)f_g}
$$
$$
= \begin{cases}
160.4 \left(\frac{e}{0.5}\right)^{0.64} \exp\left[-1.0453\, x_z^{1.581(e/0.5)^{0.177}}\right] \\
\quad \text{for} \quad 0.0005 \le \sigma_z/(1+z) < 0.005, \\
58.99 \left(\frac{e}{0.5}\right)^{0.75} x_z^{-1.6} \\
\quad \text{for} \quad 0.005 \le \sigma_z/(1+z) \le 0.02,
\end{cases}
\tag{A1}
$$

$$
\mathrm{FoM}_{P(k)}
$$
$$
= \begin{cases}
54.64 \left(\frac{e}{0.5}\right)^{0.55} \exp\left[-1.024\, x_z^{1.313(e/0.5)^{0.247}}\right] \\
\quad \text{for} \quad 0.0005 \le \sigma_z/(1+z) < 0.005, \\
19.78 \left(\frac{e}{0.5}\right)^{0.73} x_z^{-1.366} \\
\quad \text{for} \quad 0.005 \le \sigma_z/(1+z) \le 0.02,
\end{cases}
\tag{A2}
$$

where we have defined

$$
x_z \equiv \frac{\sigma_z/(1+z)}{0.005}.
\tag{A3}
$$

When Planck priors are added (see Appendix B), we find

$$
\mathrm{FoM}_{P(k)f_g}
$$
$$
= \begin{cases}
1288 \left(\frac{e}{0.5}\right)^{0.61} \exp\left[-1.815 \left(\frac{0.5}{e}\right)^{0.079} x_z^{1.464(e/0.5)^{0.06}}\right] \\
\quad \text{for} \quad 0.0005 \le \sigma_z/(1+z) < 0.005, \\
222.91 \left(\frac{e}{0.5}\right)^{0.75} x_z^{-2.165} \\
\quad \text{for} \quad 0.005 \le \sigma_z/(1+z) \le 0.02,
\end{cases}
\tag{A4}
$$

$$
\mathrm{FoM}_{P(k)}
$$
$$
= \begin{cases}
428.7 \left(\frac{e}{0.5}\right)^{0.59} \exp\left[-1.711 \left(\frac{0.5}{e}\right)^{0.103} x_z^{1.443(e/0.5)^{0.076}}\right] \\
\quad \text{for} \quad 0.0005 \le \sigma_z/(1+z) < 0.005, \\
79.9 \left(\frac{e}{0.5}\right)^{0.73} x_z^{-1.92} \\
\quad \text{for} \quad 0.005 \le \sigma_z/(1+z) \le 0.02.
\end{cases}
\tag{A5}
$$

A2 Dependence on minimum redshift

The fitting formulae of the dependence of the DETF FoM on the minimum redshift presented here correspond to the curves in right-hand panels of Fig. 2. For a slitless galaxy redshift survey only, the dependence of the FoM for (w_0, w_a) on $z_{\min}$ is well approximated by

$$
\mathrm{FoM}_{P(k)f_g} = 148.93 \left(\frac{e}{0.5}\right)^{0.68} - 237.23 \left(\frac{e}{0.5}\right)^{0.56} \Delta z_{\min}
$$
$$
\times \exp\left[-0.12 \left(\frac{\Delta z_{\min}}{0.5}\right)^3\right],
\tag{A6}
$$

$$
\mathrm{FoM}_{P(k)} = 48.26 \left(\frac{e}{0.5}\right)^{0.62} - 66 \left(\frac{e}{0.5}\right)^{0.56} \Delta z_{\min}
$$
$$
\times \exp\left[-0.05 \left(\frac{\Delta z_{\min}}{0.5}\right)^3\right],
\tag{A7}
$$

where we have defined

$$
\Delta z_{\min} \equiv z_{\min} - 0.5.
\tag{A8}
$$

When BOSS data are added, we find

$$
\mathrm{FoM}_{P(k)f_g} = 166.62 \left(\frac{e}{0.5}\right)^{0.64} - 134 \left(\frac{e}{0.5}\right)^{0.84} \Delta z_{\min},
\tag{A9}
$$

$$
\mathrm{FoM}_{P(k)} = 52.22 \left(\frac{e}{0.5}\right)^{0.59} - 56.1 \left(\frac{e}{0.5}\right)^{0.62} \Delta z_{\min}
$$
$$
\times \exp\left[-0.12 \left(\frac{\Delta z_{\min}}{0.5}\right)^3\right].
\tag{A10}
$$

For a slitless galaxy redshift survey with Planck priors (see Appendix B), we find

$$
\mathrm{FoM}_{P(k)f_g} = 1114.91 \left(\frac{e}{0.5}\right)^{0.64} - 1292.64 \left(\frac{e}{0.5}\right)^{0.48} \Delta z_{\min},
\tag{A11}
$$

$$
\mathrm{FoM}_{P(k)} = 369.58 \left(\frac{e}{0.5}\right)^{0.63} - 415 \left(\frac{e}{0.5}\right)^{0.46} \Delta z_{\min},
\tag{A12}
$$

For a slitless galaxy redshift survey combined with BOSS data and Planck priors (see Appendix B), we find

$$
\mathrm{FoM}_{P(k)f_g}
$$

$$
= \begin{cases}
1165.83 \left(\dfrac{e}{0.5}\right)^{0.62} - 817.85 \left(\dfrac{e}{0.5}\right)^{0.50} \Delta z_{\min} \\
\qquad \text{for} \quad 0.5 \leq z_{\min} \leq 0.7, \\
1002.26 \left(\dfrac{e}{0.5}\right)^{0.64} - 1155.23 \left(\dfrac{e}{0.5}\right)^{0.82} (z_{\min} - 0.7) \\
\qquad \text{for} \quad 0.7 < z_{\min} \leq 1,
\end{cases} \tag{A13}
$$

$$
\mathrm{FoM}_{P(k)} = \begin{cases}
386.53 \left(\dfrac{e}{0.5}\right)^{0.61} - 264.35 \left(\dfrac{e}{0.5}\right)^{0.44} \Delta z_{\min} \\
\qquad \text{for} \quad 0.5 \leq z_{\min} \leq 0.7, \\
333.66 \left(\dfrac{e}{0.5}\right)^{0.63} - 400.27 \left(\dfrac{e}{0.5}\right)^{0.58} (z_{\min} - 0.7) \\
\qquad \text{for} \quad 0.7 < z_{\min} \leq 1.
\end{cases} \tag{A14}
$$

A3 Dependence on the Hα flux limit

The fitting formulae of the dependence of the DETF FoM on the Hα flux limit presented here correspond to the curves in left-hand panels of Fig. 3. For slitless galaxy redshift surveys, the dependence of the FoM for (w_0, w_a) on the Hα flux limit is well approximated by

$$
\mathrm{FoM}_{P(k)f_g} = 148.9 \left(\frac{e}{0.5}\right)^{0.68} \exp\left[-0.321 \left(\frac{0.5}{e}\right)^{0.37} (\bar{f} - 4)\right], \tag{A15}
$$

$$
\mathrm{FoM}_{P(k)} = 48.3 \left(\frac{e}{0.5}\right)^{0.62} \exp\left[-0.275 \left(\frac{0.5}{e}\right)^{0.4} (\bar{f} - 4)\right], \tag{A16}
$$

where $\bar{f} \equiv f/[10^{-16}\,\mathrm{erg\,s^{-1}\,cm^{-2}}]$. When Planck priors (see Appendix B) are added to slitless galaxy redshift surveys (not shown in Fig. 3), we find

$$
\mathrm{FoM}_{P(k)f_g} = 1114.9 \left(\frac{e}{0.5}\right)^{0.64} \exp\left[-0.288 \left(\frac{0.5}{e}\right)^{0.37} (\bar{f} - 4)\right], \tag{A17}
$$

$$
\mathrm{FoM}_{P(k)} = 369.6 \left(\frac{e}{0.5}\right)^{0.63} \exp\left[-0.273 \left(\frac{0.5}{e}\right)^{0.39} (\bar{f} - 4)\right]. \tag{A18}
$$

A4 Dependence on *H*-band magnitude limit

The fitting formulae of the dependence of the DETF FoM on the *H*-band magnitude limit presented here correspond to the curves in the right-hand panels of Fig. 3. For multislit galaxy redshift surveys, the dependence of the FoM for (w_0, w_a) on the *H*-band magnitude limit can be approximated by

$$
\mathrm{FoM}_{P(k)f_g}
$$
$$
= 367.5 \left(\frac{e}{0.315}\right)^{0.47} + 565.6 \left(\frac{e}{0.315}\right)^{0.43} (H_{AB} - 22), \tag{A19}
$$

$$
\mathrm{FoM}_{P(k)}
$$
$$
= 89.7 \left(\frac{e}{0.315}\right)^{0.38} + 97.1 \left(\frac{e}{0.315}\right)^{0.36} (H_{AB} - 22). \tag{A20}
$$

Note that for multislit surveys, e is the product of the redshift efficiency and the redshift sampling rate. Thus for a redshift efficiency of 90 per cent, and a redshift sampling rate of 35 per cent, $e = 0.315$.

When Planck priors (see Appendix B) are added to multislit galaxy redshift surveys (not shown in Fig. 3), we find

$$
\mathrm{FoM}_{P(k)f_g}
$$
$$
= 1907.6 \left(\frac{e}{0.315}\right)^{0.4} \exp\left[0.71 \left(\frac{e}{0.315}\right)^{0.23} (H_{AB} - 22)\right], \tag{A21}
$$

$$
\mathrm{FoM}_{P(k)}
$$
$$
= 576.4 \left(\frac{e}{0.315}\right)^{0.37} \exp\left[0.64 \left(\frac{e}{0.315}\right)^{0.34} (H_{AB} - 22)\right]. \tag{A22}
$$

APPENDIX B: PLANCK PRIORS

We derive and include Planck priors as discussed in Mukherjee et al. (2008). Our simulation and treatment of Planck data is as in Pahud et al. (2006). We include the temperature and polarization (TT, TE and EE) spectra from three temperature channels with specification similar to the HFI channels of frequency 100, 143 and 217 GHz, and one 143-GHz polarization channel, following the current Planck documentation.[10] The full likelihood is constructed assuming a sky coverage of 0.8. We choose a fiducial model to be the EUCLID fiducial model: $\Omega_m = 0.25$, $\Omega_\Lambda = 0.75$, $h = 0.7$, $\sigma_8 = 0.80$, $\Omega_b = 0.0445$, $w_0 = -0.95$, $w_a = 0$ and $n_s = 1$.

CMB data can be effectively and simply summarized in the context of combining with other data by adding a term in the likelihood that involve the CMB shift parameter R, the angular scale of the sound horizon at last scattering l_a, the baryon density $\Omega_b h^2$ and the power-law index of the primordial matter power spectrum n_s (Wang & Mukherjee 2006, 2007). This method is independent of the dark energy model used as long as only background quantities are varied. The CMB shift parameter R is defined as

$$
R \equiv \sqrt{\Omega_m H_0^2}\, r(z_{CMB}), \quad l_a \equiv \pi r(z_{CMB})/r_s(z_{CMB}), \tag{B1}
$$

where $r(z)$ is the comoving distance from the observer to redshift z, and $r_s(z_{CMB})$ is the comoving size of the sound horizon at decoupling.

The comoving distance to a redshift z is given by

$$
r(z) = c H_0^{-1} |\Omega_k|^{-1/2} \mathrm{sinn}[|\Omega_k|^{1/2}\, \Gamma(z)],
$$
$$
\Gamma(z) = \int_0^z \frac{dz'}{E(z')}, \qquad E(z) = H(z)/H_0, \tag{B2}
$$

where $\Omega_k = -k/H_0^2$ with k denoting the curvature constant, and $\mathrm{sinn}(x) = \sin(x), x, \sinh(x)$ for $\Omega_k < 0$, $\Omega_k = 0$ and $\Omega_k > 0$, respectively, and

$$
E(z) = \left[\Omega_m(1+z)^3 + \Omega_{rad}(1+z)^4 + \Omega_k(1+z)^2 + \Omega_X X(z)\right]^{1/2}, \tag{B3}
$$

with $\Omega_X = 1 - \Omega_m - \Omega_{rad} - \Omega_k$, and the dark energy density function $X(z) \equiv \rho_X(z)/\rho_X(0)$.

---

[10] www.rssd.esa.int/index.php?project=PLANCK&page=perf_top

We calculate the distance to decoupling, z_{CMB}, via the fitting formula in Hu & Sugiyama (1996) (same as that used by CAMB; Lewis, Challinor & Lasenby 2000). The comoving sound horizon at recombination is given by

$$r_s(z_{CMB}) = \int_0^{t_{CMB}} \frac{c_s \, dt}{a} = c H_0^{-1} \int_{z_{CMB}}^{\infty} dz \, \frac{c_s}{E(z)}$$

$$= c H_0^{-1} \int_0^{a_{CMB}} \frac{da}{\sqrt{3(1 + \overline{R_b}\, a)\, a^4 E^2(z)}}, \qquad (B4)$$

where a is the cosmic scale factor, $a_{CMB} = 1/(1 + z_{CMB})$, and $a^4 E^2(z) = \Omega_{rad} + \Omega_m a + \Omega_k a^2 + \Omega_X X(z) a^4$. The radiation density is computed using the Stefan–Boltzmann formula from the CMB temperature, assuming 3.04 families of massless neutrinos. The sound speed is $c_s = 1/\sqrt{3(1 + \overline{R_b}\, a)}$, with $\overline{R_b}\, a = 3\rho_b/(4\rho_\gamma)$, $\overline{R_b} = 31\,500\, \Omega_b h^2 (T_{CMB}/2.7\,\mathrm{K})^{-4}$.

We derived the full covariance matrix of $(R, l_a, \Omega_b h^2, n_s)$ through a Markov chain Monte Carlo (MCMC) based likelihood analysis (Lewis & Bridle 2002) of simulated Planck data. The Fisher matrix of $\boldsymbol{q} = (R, l_a, \omega_b, n_s)$ is the inverse of the covariance matrix of $\boldsymbol{q}$. Note that the CMB shift parameters R and l_a encode all the information on dark energy parameters. For any given dark energy model parameterized by the parameter set $\boldsymbol{p}_X$, the relevant Fisher matrix for $\boldsymbol{p} = (\boldsymbol{p}_X, \Omega_X, \Omega_k, \omega_m, \omega_b, n_s)$ can be found using equation (10). Equation (11) and Section 3.7 describe our dark energy parametrization.

This paper has been typeset from a TeX/LaTeX file prepared by the author.